Applied Physics A (2023) 129:411
https://doi.org/10.1007/s00339-023-06699-7

Applied Physics A
Materials Science & Processing

Environment friendly and non-toxic flexible Bi_2O_2S nanosheet photodetector based on deionized water solid electrolyte

Ganbo Zhang[1] · Nanyin Zhao[1] · Kai Wang[1] · Jun Li[1]

Received: 1 February 2023 / Accepted: 4 May 2023 / Published online: 12 May 2023

Abstract

Researchers are already becoming willing to get involved in bismuth oxysulfide (Bi_2O_2S), a new two-dimensional optoelectronic material with a lengthy carrier lifetime and a unique loose structure. In this work, the Bi_2O_2S nanosheets are produced by room temperature chemical synthesis and built a Bi_2O_2S nanosheets flexible photodetector based on deionized water solid-state electrolytes. Photoelectrochemical tests showed that the photodetector based on deionized water solid-state electrolyte had excellent photoresponse performance under 0 V, and its photocurrent density was 0.55 μA/cm^2 when the optical power was 75 mW/cm^2. In addition, the photodetector exhibited superb stability. After cycling the "on–off" behavior for 1000 s, the photocurrent slightly decreased 8% than initial state. At a bending angle of 30°, the photocurrent density was about 91% of the original state, but when the bending angle is 60°, the photocurrent density was about 76% of the original state, which may be caused by the small cracks formed during the bending process. The results showed that the flexible photodetector based on Bi_2O_2S nanosheets had decent stability and mechanical flexibility, and were safer and more environmentally friendly than traditional detectors, providing a workable option for the flexible photodetector's construction.

Keywords Bi_2O_2S nanosheets · Flexible photodetectors · Photoelectrochemical photodetector · Solid-state electrolyte

1 Introduction

Photoelectric detection has been commonly used in a range of industries [1–5], encompassing biological imaging, medical, military, information, and energy. The majority of today's commercial photodetectors are built on stiff silicon and germanium substrates, which have suffered several disadvantages such as being unpredictable, unbendable, and vulnerable. In contrast, the flexible photodetector has the advantages of being small in size, lightweight, bendable and convenient to carry, which is more in line with the development prospects of the photodetector. The mechanical ductility of traditional two-dimensional materials on the flexible substrate is relatively poor, and the overall stability depends on the rigidity of the substrate, which limits the development in the field of flexibility. As a result, scientists are eager to discover novel materials with superior mechanical flexibility, tunable bandgap, strong light absorption, and simple preparation for flexible substrates.

Two-dimensional (2D) materials [6, 7] had turned into the material of decision for flexible photodetectors because of their smaller expense, adjustable bandgap, excellent electronic transmission characteristics, great mechanical flexibility, and excellent optical properties [8–12]. Be that as it may, conventional two-dimensional materials such as graphene [13] do not have bandgap and limits of light absorption, transition metal dichalcogenides (TMDs) [11, 14] and black phosphorous (BP) [15] require complex packaging and numerous different problems restrict the advancement of the materials on flexible substrates. In recent years, a narrow bandgap layered Bi_2O_2Se [16–18] consisting of cation $[Bi_2O_2]_n^{2n+}$ and anion $[Se]_n^{2n-}$ has entered the research neighborhood. It has excellent air stability and high electron mobility (> 20 000 cm^2 V^{-1} s^{-1} at 2 K), long carrier life, high electron hole decomposition efficiency and adjustable bandgap which has stimulated researchers' interest in bismuth oxygen chalcogenide (Bi_2O_2X (X = Bi, S, Te)) [19–22] because of these excellent properties. Huang et al. discovered that doping Bi_2O_2S could extend the life of solar

✉ Jun Li
lijun@xtu.edu.cn

[1] Hunan Provincial Key Laboratory of Micro-Nano Energy Materials and Devices and School of Physics and Optoelectronics, Xiangtan University, Hunan 411105, People's Republic of China

cells and increase battery performance [23], and Zhang et al. discovered that lowering the dimensionality of Bi_2O_2S could improve thermoelectric performance [24]. By analyzing the atomic structure of Bi_2O_2S, it is found that the Bis donor defect is dominant, leading to the introduction of n-type carrier in Bi_2O_2S [25–28]. Furthermore, a decent bandgap (1.5 eV) and orthorhombic crystal structure, as well as a low crystal accumulation factor (PF = 0.66) give a vast space for atom vibration, resulting in a bigger Bohr radius and a longer carrier lifetime for Bi_2O_2S [29, 30].

Photodetectors have been studied in more detail to improve their performance and manufacturing process [31]. Photodetectors with flexible substrates have two key advantages: first, they have better mechanical resilience; second, the production process is simple, low cost, and more suitable for use in daily life [32]. Whether the photodetector is based on a rigid or flexible base, an emergency outage will occur. However, photochemical (PEC) photodetectors can operate without external bias [33]. The working properties of the photochemical-type photodetectors are similar to those of the Schottky junction photovoltaic photodetectors. The essence of the Schottky junction photodetectors is that the two materials have different work functions which cause the diffusion of charge carriers. In the photochemical-type detector, these two materials are electrolyte and electrode materials respectively. Bellani and his colleagues created PET-type photodetectors [34] with GeSe nanoflakes as the active material that had fallen off from the liquid phase. The photocurrent density of the GeSe photocathode could reach 10.9 A cm^{-2} without an external bias, 0.5 mol/L H_2SO_4 electrolyte, and 455 nm excitation wavelength, and the response rate and external quantum efficiency were 0.32 A W^{-1} and 86.3%, respectively. Renet et al. also created black phosphorous nanosheets for photoelectrochemical photodetectors' electrode fabrication. The constructed photodetectors displayed a photocurrent density of 265 nA under a 100 mW cm^{-2} irradiation [35]. In addition, traditional PEC photodetectors have some defects, such as leakage of packaging liquid and large device size and material attached to a rigid substrate, which limits their development in this field. However, the combination of solid-state electrolytes and active materials is an excellent solution to these problems, mainly because solid-state electrolytes are more stable, more malleable, and have excellent ionic conductivity than liquid electrolytes [36] and the combination of the two can be better attached to the flexible substrate. Therefore, the solid-state electrolyte based on PEC flexible photodetector is an upgraded version of the traditional PEC photodetector [37–39].

In this study, we synthesized Bi_2O_2S nanosheets using a one-pot wet-chemical synthesis process and constructed a photodetector based on Bi_2O_2S. The photoresponse and mechanical flexibility of Bi_2O_2S photodetector were tested in neutral and solid-state electrolytes. Finally, the experimental results showed that the device had good light response performance and remarkable environmental stability. Because the equipment has the advantages of low cost, lightweight and easy carrying, this study has reference value for the development of flexible equipment.

2 Experimental section

2.1 The preparation process of materials

To prepare Bi_2O_2S nanosheets, 100 mg of bismuth nitrate pentahydrate was poured into beaker A with 20 mL of deionized water in the first step, and beaker A was placed under ultrasonic treatment to make the internal mixture more uniform until all dissolved. Left beaker A for a while and no precipitation was produced. The materials were fully mixed after 1 mL of hydrazine hydrate and 12.7 mg of thiourea were mixed and placed in beaker B, which was exposed to ultrasonic treatment for 2 h. After mixing the solutions in beakers A and B, 120 mg potassium hydroxide and 320 mg sodium hydroxide were added for stirring. Afterward, the solution was observed to change color from milky white to brown. Stirred the mixture continuously for 30 min and stood overnight. Collected the dark precipitate, washed it with water and alcohol at least 5 times, and then dried it in a 70-degree vacuum drying oven. The specific preparation process is shown in Fig. 1.

2.2 Preparation of solid-state electrolytes

The solid-state electrolyte was prepared by adopting the previously reported water bath method [40]. Of which, the neutral solid-state electrolyte was to add 1.5 g polyvinyl alcohol (PVA, 1.5 g, Qingdao YouSuo Chemical Technology Co., Ltd.) to the beaker containing 16 mL of deionized water and the KOH solid-state electrolyte also requires an additional 1 g of potassium hydroxide (KOH, 1 g, Analysis of pure, Hunan HuiHong Reagent Co., Ltd.). To make a translucent colloid, place the mixed solution in a water bath stirring furnace and stir rapidly at 95 °C for 20 min. Polyvinyl alcohol is a kind of polymer organic compound, odorless, non-toxic, no irritation to human body. Potassium hydroxide is highly corrosive and will cause certain impact on human body and environment. Alkaline solid electrolytes were not used in this work, and the alkaline solid electrolytes mentioned in the paper are only to enrich the types of solid electrolytes. Therefore, this work is still in line with the concept of environmental protection and non-toxic.

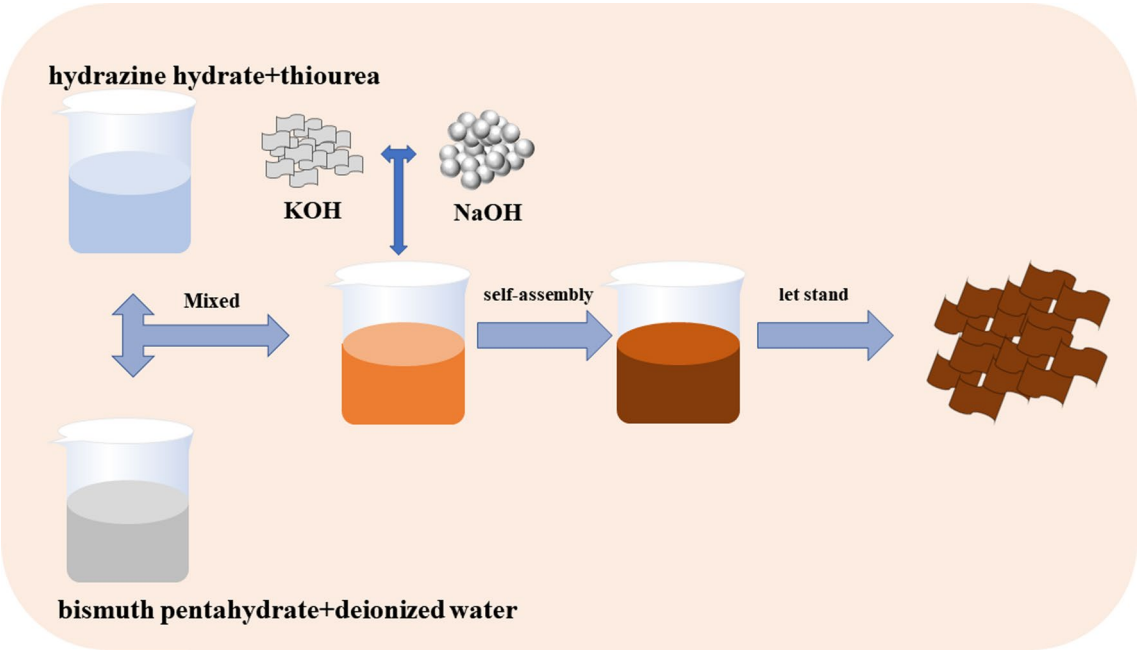

Fig. 1 The schematic of the synthesis of Bi_2O_2S nanosheets

2.3 Device fabrication and measurements

On an ethylene terephthalate (PET) substrate, a flexible photodetector based on Bi_2O_2S was constructed. To obtain a consistent suspension, we added 1 mg of Bi_2O_2S to 1 mL of alcohol and used an ultrasonic treatment. Used a dropper, and dropped the prepared suspension onto the PET substrate. To make a carbon black solution, 1 mg carbon black was mixed with 1 mL NMP (*N*-Methyl-2-pyrrolidone), and 200 µL of the carbon black solution were dropped on the PET substrate. The two substrates were dried for 8 h in a vacuum drying oven at 60 °C. After the substrate was fully dried, the solid electrolyte was uniformly covered on the PET substrate containing Bi_2O_2S nanosheets, and then the PET substrate containing carbon black was covered on the Bi_2O_2S nanosheets substrate and dried at room temperature for 4 h, and finally, the flexible device was obtained. The specific assembly schematic diagram is shown in Fig. 2a.

In this article, the photoelectric performance test was carried out in a photoelectrochemical workstation (CHI660D, Chen Hua, China). The working electrode was placed in the PET substrates that had been coated with Bi_2O_2S nanosheets, while the reference and counter electrodes were sandwiched in the PET substrates that had been coated with carbon black. The scan rate in the linear volt-ampere characteristic (LSV) test was 10 mV/s. The period of the current–time relationship (*i*–*t*) curve was 20 s, the test light source was a 350 W xenon lamp (CEL-HXF300/CEL-HXUV300, 190–1100 nm), and a radiometer was utilized to objectively examine the varied powers.

2.4 Materials' characterizations

A Scanning Electron Microscope was used to examine the morphology of the produced Bi_2O_2S nanosheets (SEM, ZEISS, Sigma300). The distinctive peaks of Bi_2O_2S nanosheets were seen using Cu K radiation X-ray diffraction (XRD). Following that, a Raman microscope was used to perform Raman measurements to investigate the micro-mechanics of Bi_2O_2S (Renishaw, In Via). Finally, the absorption range of Bi_2O_2S nanosheets was analyzed by ultraviolet–visible spectrometer (SHIMADZU UV-2600i).

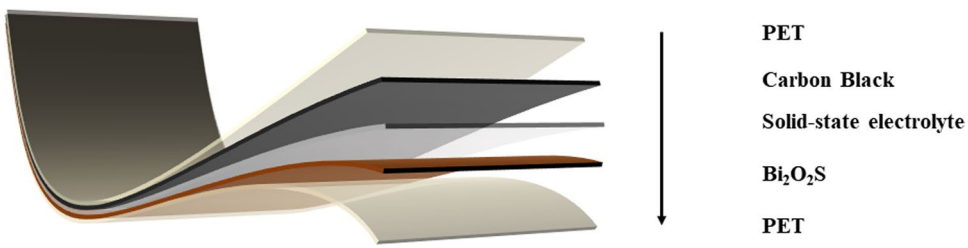

Fig. 2 Preparation process of flexible photodetectors based on Bi_2O_2S nanosheets

3 Results and discussion

The synthesis roadmap was described in detail in the experimental section. The loosely stacked structure was confirmed by analyzing the atomic structure simulation diagram of Bi_2O_2S in Fig. 3a. To confirm the formation of the material, we performed a Raman analysis on Bi_2O_2S, and the results of the Raman analysis are shown in Fig. 3b. We could clearly see several spikes through the Raman diagram, corresponding to the external manifestations of the B_{2g}, A_{1g}, and B_{1g} vibrational modes of Bi_2O_2S, which were consistent with previous reports. To further confirm the synthesis of the material, the prepared Bi_2O_2S nanosheets were characterized by an X-ray diffractometer

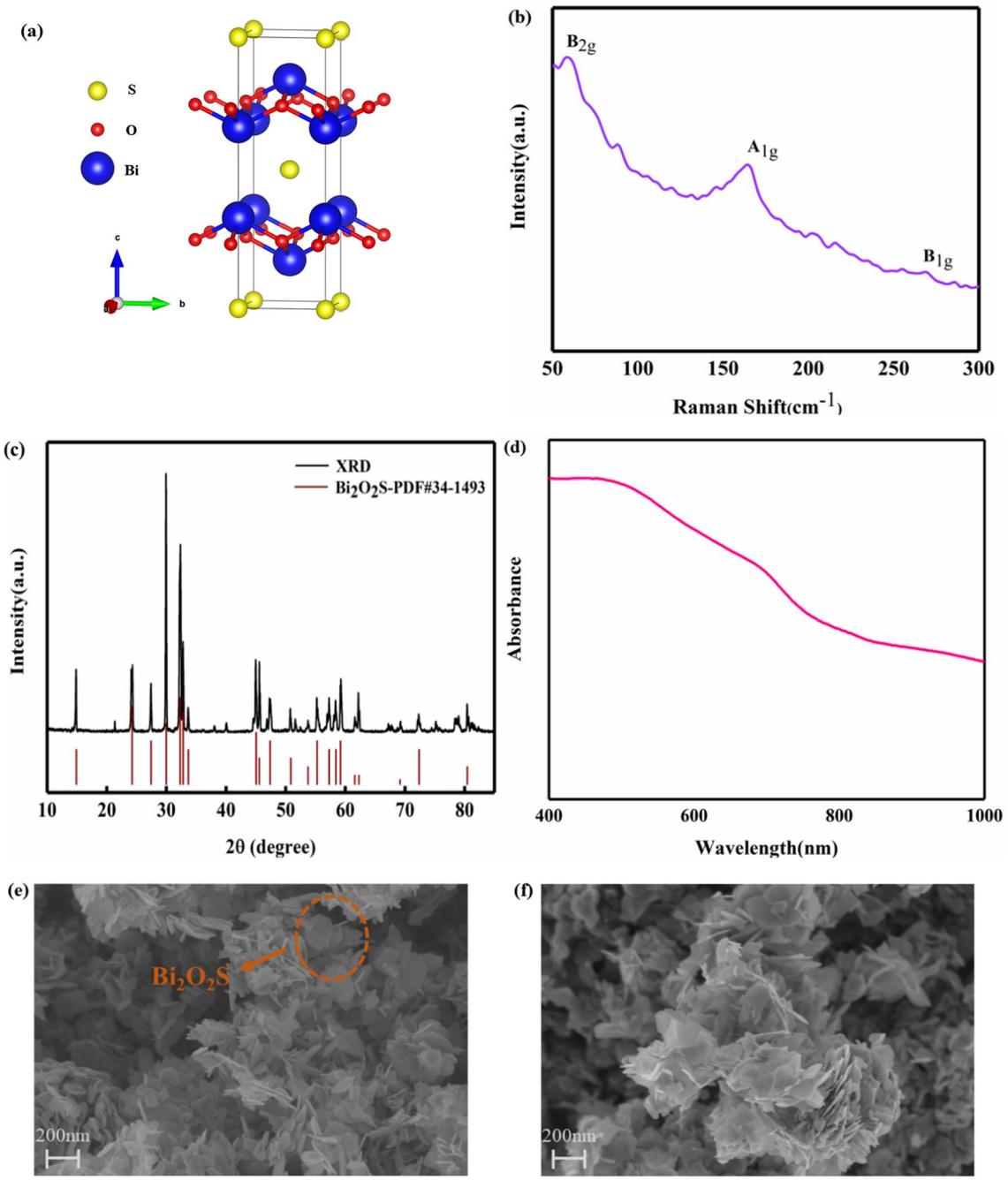

Fig. 3 **a** The atomic structure model diagram of Bi_2O_2S. **b** The Raman measurement of Bi_2O_2S. **c** The XRD pattern of Bi_2O_2S. **d** UV–Visible absorption spectrum. **e** and **f** SEM of Bi_2O_2S nanosheets

(XRD). Figure 3c shows the comparison of the X-ray diffraction pattern and the Bi_2O_2S standard card. The comparison of the X-ray diffraction pattern and the standard card showed that the diffraction peaks were consistent with those of the standard card, the diffraction peaks were very sharp and there were no excessive burrs in the pattern, which indicates that the Bi_2O_2S nanosheets had a high crystallinity. In addition, Fig. 3d shows the absorption spectrum of Bi_2O_2S nanosheets, where a strong absorption in the visible range could be observed, indicating its potential for solar energy applications. Therefore, all tests in this work were performed in the simulated solar range. Finally, the Bi_2O_2S nanosheets were characterized by scanning electron microscopy. It could be clearly observed from Fig. 3e and f that the material had an obviously layered structure. The characterization results showed that we had successfully synthesized Bi_2O_2S nanosheets.

We ran a complete test on the flexible photodetector based on Bi_2O_2S nanosheets under a photoelectrochemical workstation to evaluate its light response performance. Figure 4a illustrates the LSV curve of Bi_2O_2S. The current expanded as the applied voltage was enhanced, regardless of whether the current was measured in simulated sunlight or dark settings, as shown in Fig. 4a. This was since when a potential is applied, a potential gradient was formed inside the Bi_2O_2S, resulting in the formation of an electric field, but the applied bias may initially cancel with the built-in electric field. Electrons could only be transported to the cathode or react with the scavenger indicated by the electrode when an electric field is applied [41]. This method enhanced electron–hole pair separation while less electron–hole pair recombination efficiency. In the 0–1 V procedure, no apparent redox peaks were identified, indicating that Bi_2O_2S was more stable. In addition, the Bi_2O_2S flexible photodetector based on solid-state electrolytes similarly displays a significant optical response without adding any bias voltage, which indicates the potential of the device to be self-powered, as shown in Fig. 4b. Therefore, the following tests were performed at 0 V. Solid electrolytes prepared based on deionized water were used in Bi_2O_2S flexible photodetector, which is also very consistent with the concept of environmental protection.

Additionally, the bias voltage and the incident light intensity was also important parameter that had a significant impact on the photodetector's performance and the research's importance was self-evident. It simulated two cases, one in sunlight and another in darkness, with 20 s as the on-and-off frequency time. The power was evaluated from 55 to 95 mW/cm^2 at 0 V bias, respectively. A flexible photodetector with a solid-state electrolyte is shown in Fig. 5a. Under the forward light intensity, the photocurrent density was from 0.5 to 1 μA/cm^2. The photocurrent density increased by about two times. Figure 5b shows the photocurrent intensity of the Bi_2O_2S flexible photodetector

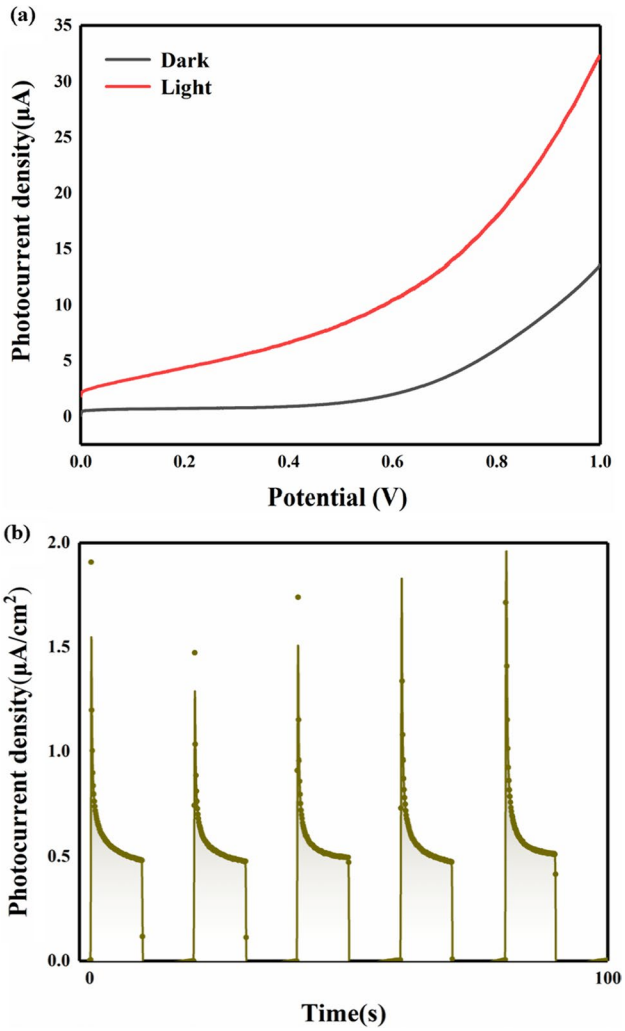

Fig. 4 **a** The LSV curves of the photodetector based on Bi_2O_2S nanosheets. **b** Photocurrent density at 0 V with 75 mW/cm^2

at different bias voltages. We can see from the figure that the overall trend is rising, which is in line with the trend of LSV curve. However, when the bias voltage increases from 0.3 to 0.4 V, the increase in photocurrent density is relatively large. The reason may be that the increase of bias voltage leads to the ionization of deionized water in solid electrolyte, thus increasing the ion concentration.

In order to further investigate the photoresponse performance of the Bi_2O_2S flexible photodetector, the relationship was extracted by analyzing the *i*–*t* plot and a relationship plot between optical power density, photocurrent and photoresponse was generated to further understand the photoresponse performance of the Bi_2O_2S flexible photodetector. The linear relationship presented in the graph implies that the material was well crystalline [38]. Response time was an important indicator of a photodetector's performance and was defined as how long it took for the photocurrent

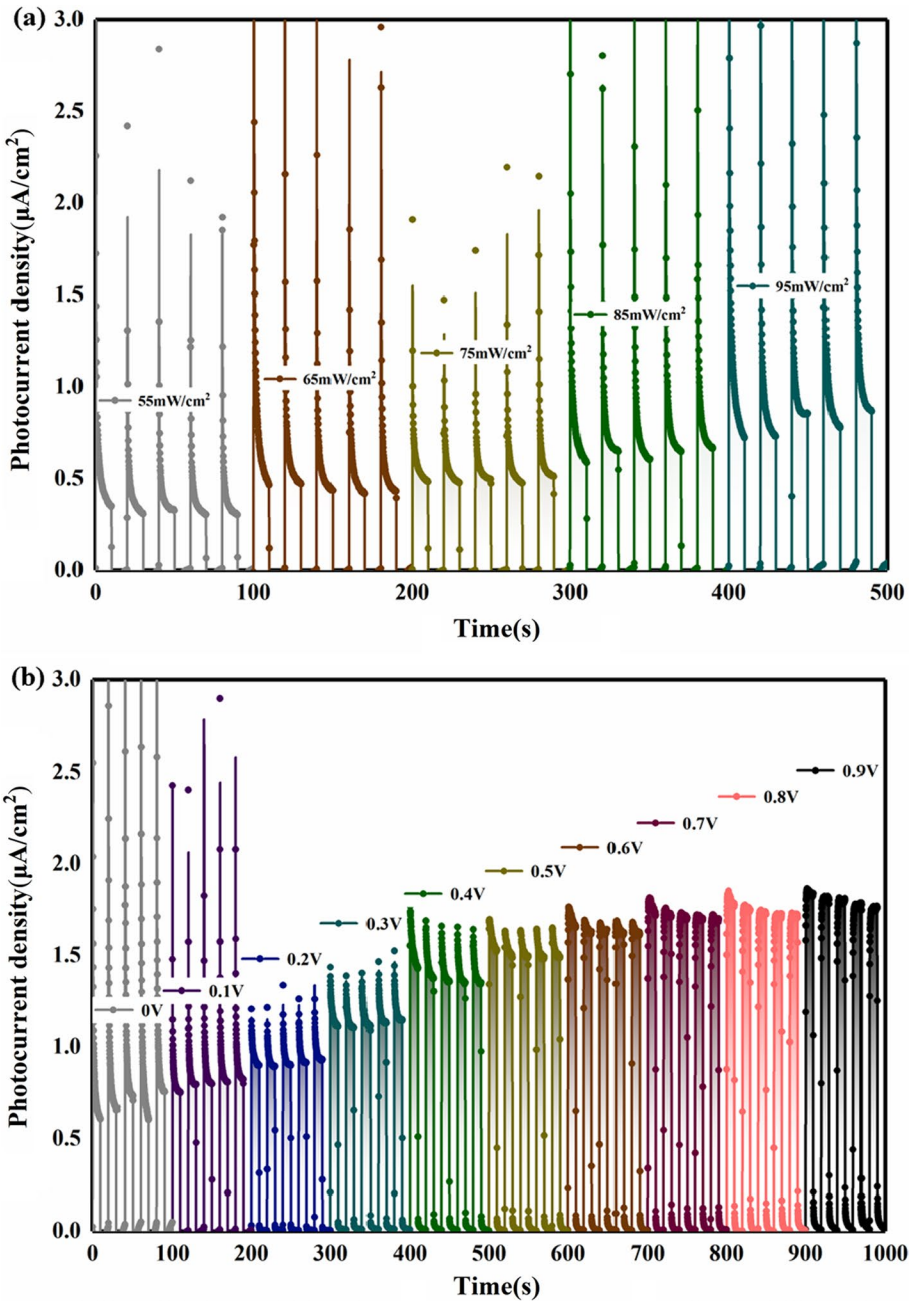

Fig. 5 **a** is the photocurrent intensity of the flexible photodetector based on neutral solid electrolyte under different light intensities. **b** is the photocurrent intensity of the flexible photodetector based on neutral solid electrolyte under different bias voltages

to rise from 10 to 90% and it took to fall from 90 to 10%, respectively. Figure 6a , b shows the rise time and fall time of photodetectors based on solid-state electrolytes at 75 mW/cm^2 without any bias applied. As shown in Tables 1 and 2, by comparing the response time of the traditional photodetector and the flexible photodetector, it can be seen that the detector has a super-fast response rate. Nonetheless, analysis of the curve reveals that the fall time was generally more than the rise time, which was primarily due to the temperature. Photogenerated carriers were generated when the light was shone on the Bi_2O_2S electrode, and the temperature of the electrode increased leading to carrier life being extended at the same time. In addition, the photoresponse rate R under varied incident light power was also calculated, revealing the photocurrent generated by the incident light per unit power in the effective area, the specific formula is: $R = (I_{ligh} - I_{dark})/P^*S$, where I_{light} was photocurrent, I_{dark} was dark current, P was light intensity, and S was effective light area. As shown in Fig. 6c, the photoresponse coefficient of the Bi_2O_2S flexible photodetector varies from 6.9 to 10.2 μA/W under solid-state electrolyte and without bias conditions.

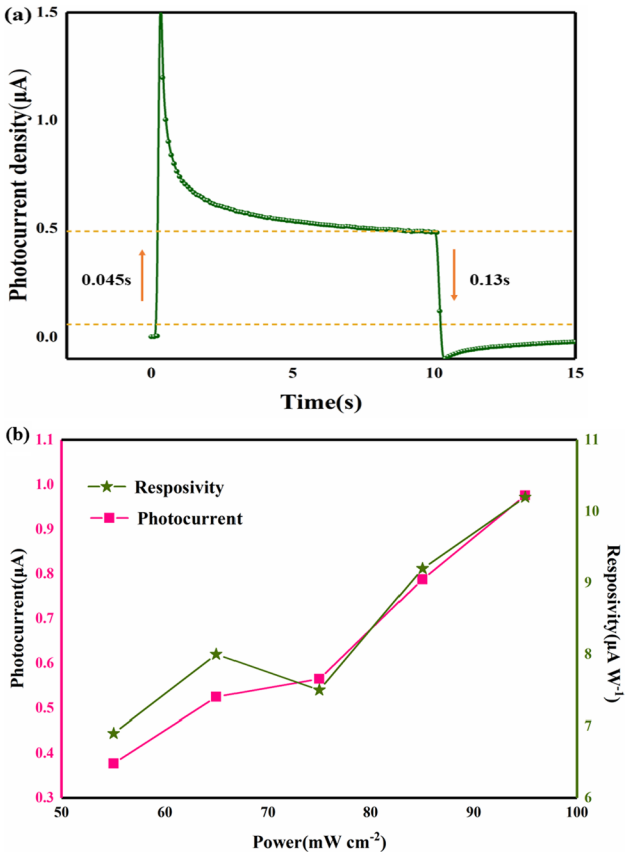

Fig. 6 **a** Response time at a bias of 0 V and a light intensity of 75 mW/cm^2. **b** The relationship between the photocurrent, photoresponse, and optical power density of Bi_2O_2S nanosheets under the conditions of deionized water solid electrolyte

To analyze the mechanical strain capability of the Bi_2O_2S photodetector, we conducted performance tests in three different states without bias, and the detailed test results are shown in Fig. 7a. It could be seen from the figure that there is no significant change in performance when the angle changed from 0° to 30°, and there was a drop in current when it switched from 30° to 60°, and the dropping may be due to the bending of the PET substrate was leading to an imbalance between the central pressure and the two sides were generating some cracks in the middle of the Bi_2O_2S electrode. The results of the mechanical strain test demonstrated that the device had some resistance to bending and stability.

Eventually, it was well known that stability was an important indicator to judge the performance of photodetectors and to test whether they could be employed effectively in real life. Accordingly, we conducted stability tests on the Bi_2O_2S flexible photodetector. As shown in Fig. 7b, the cyclic stability was tested in the state without any external bias. The results indicated that after cycling the test for 1000 s with no bias voltage, the performance decreases by 8% from the initial state, but is still within the limit. The decline in performance may be due to structural damage caused by prolonged exposure to light, and the Bi_2O_2S nanosheets fuse with each other to form a polymer [50]. In summary, the solid-state electrolyte-based Bi_2O_2S self-powered photodetector had a kind photoresponse performance and fabulous stability.

Table 1 Comparison with other detectors

Material	Measurement condition	Wavelength (nm)	Response time (s)	Responsivity (μA/W)	References
Bi_2O_2S nanoplates	Solid-state electrolyte, 0 V	White	0.045	10.2	This work
Bi QDs	0.1 M KOH 0.6 V	White	0.2	8.64	[42]
Sb NSs	0.5 M KOH 0.6 V	White	1	1.5	[43]
Te NSs	0.1 M KOH 0.6 V	White	0.055	1.16	[44]
InSe NSs	0.2 M KOH 1 V	White	7	3.3	[45]
GeSe NSs	0.1 M KOH 0.3 V	UV–Visible	0.2	43.6	[46]

Table 2 Comparison with other flexible detectors

Material	Measurement condition	Wavelength (nm)	Response time (s)	References
Bi_2O_2S nanoplates	Solid-state electrolyte, 0 V	White	0.045	This work
WS_2-graphene nanoplates	H_2SO_4 solid-state electrolyte, 0 V	White	2.3	[47]
LSG/$CsPbBr_3$	PET, 0 V	532 nm	0.03	[48]
$FePS_3$/rGO	Solid-state electrolyte, 0 V	White	0.2	[49]

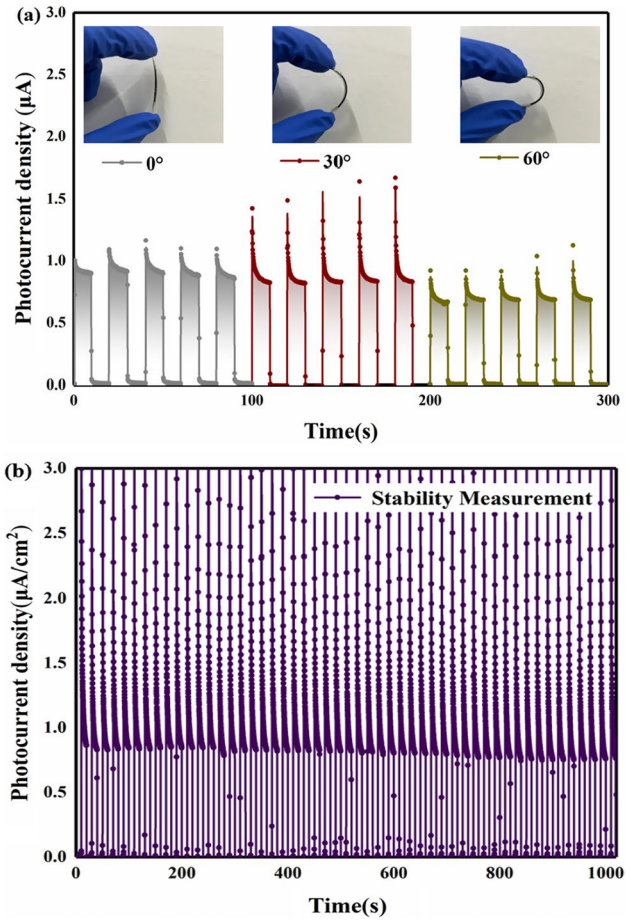

Fig. 7 **a** Under the same conditions, the photocurrent density for different bending angles. **b** Comparison of the current density of Bi_2O_2S nanosheets photodetector after 1000 s of cyclic test and initial test time

4 Conclusions

As previously stated, in our work, Bi_2O_2S nanosheets were successfully synthesized at room temperature, and a flexible photodetector based on deionized water solid-state electrolyte was constructed utilizing Bi_2O_2S nanosheets. The prepared Bi_2O_2S flexible photodetector exhibited decent light response, great mechanical flexibility, and fabulous environmental stability during the test and were environmentally friendly, non-toxic, and consistent with sustainable development. At 0 V, the responsivity could reach 10.2 μA/W and the response speed reaches 0.045 s. When a bending angle of 30°, the photocurrent intensity decreased by only 8%, and the photocurrent remains stable after 1000 s of "on–off" behavior. In addition, the device had the advantages of small size, lightweight, and portability, and had greater potential in wearable photodetectors and low-power photovoltaic applications. Thus, this work could promote the progress of flexible optoelectronic devices based on solid-state electrolytes.

Acknowledgements This work was supported by the Scientific Research Fund of Hunan Provincial Education Department (No. 22B0171, 19C1746), National Basic Research Program of China (No. 2015CB921103), and the Program for Changjiang Scholars and Innovative Research Team in University (IRT 17R91), Natural Science Foundation of Hunan Province (No. 2021JJ40524).

Author contributions GZ: conceptualization, methodology, validation, investigation, formal analysis, data curation, writing—original draft, visualization. NZ: resources, investigation. KW: writing—review and editing, supervision. JL: conceptualization, writing—review and editing.

Data availability The data that support the findings of this study are available from the corresponding author upon reasonable request.

Declarations

Conflict of interest The authors are aware of the ethical responsibilities and the manuscript has no conflict of interest.

References

1. F. Wang, Y. Zhang, Y. Gao et al., 2D metal chalcogenides for IR photodetection. Small **15**(30), 1901347 (2019)
2. C.-H. Liu, Y.-C. Chang, T.B. Norris et al., Graphene photodetectors with ultra-broadband and high responsivity at room temperature. Nat. Nanotechnol. **9**(4), 273–278 (2014)
3. A.D. Iacovo, C. Venettacci, L. Colace et al., PbS colloidal quantum dot visible-blind photodetector for early indoor fire detection. IEEE Sens. J. **17**, 4454–4459 (2017)
4. A.J. Makynen, J.T. Kostamovaara, T.E. Rahkonen, CMOS photodetectors for industrial position sensing. IEEE Trans. Instrum. Meas. **43**(3), 489–492 (1994)
5. F. González-Posada, R. Songmuang et al., Environmental sensitivity of n-i-n and undoped single GaN nanowire photodetectors. Appl. Phys. Lett. **102**(21), 213113 (2013)
6. S.Z. Butler, S.M. Hollen, L. Cao et al., Progress, challenges, and opportunities in two-dimensional materials beyond graphene. ACS Nano **7**(4), 2898–2926 (2013)
7. Q.H. Wang, K. Kalantar-Zadeh, A. Kis et al., Electronics and optoelectronics of two-dimensional transition metal dichalcogenides. Nat. Nanotechnol. **7**(11), 699–712 (2012)
8. S. Xia, Y. Diao, C. Kan, Electronic and optical properties of two-dimensional GaN/ZnO heterojunction tuned by different stacking configurations. J. Colloid Interface Sci. **607**, 913–921 (2022)
9. P. Tian, H. Wu, L. Tang et al., Ultrasensitive broadband photodetectors based on two-dimensional Bi2O2Te films. J. Mater. Chem. C **9**(39), 13713–13721 (2021)
10. J. Yin, Z. Tan, H. Hong et al., Ultrafast and highly sensitive infrared photodetectors based on two-dimensional oxyselenide crystals. Nat. Commun. **9**(1), 3311 (2018)
11. O. Lopez-Sanchez, D. Lembke, M. Kayci et al., Ultrasensitive photodetectors based on monolayer MoS_2. Nat. Nanotechnol. **8**(7), 497–501 (2013)
12. F.H.L. Koppens, T. Mueller, P. Avouris et al., Photodetectors based on graphene, other two-dimensional materials and hybrid systems. Nat. Nanotechnol. **9**(10), 780–793 (2014)
13. Y. Wu, C. Cao, C. Qiao et al., Bandgap-tunable phosphorus-doped monolayer graphene with enhanced visible-light photocatalytic H-2-production activity. J. Mater. Chem. C **7**(34), 10613–10622 (2019)
14. S.-Y. Kim, J. Kwak, C.V. Ciobanu et al., Recent developments in controlled vapor-phase growth of 2D group 6 transition metal dichalcogenides. Adv. Mater. **31**(20), 1804939 (2019)

15. Y. Zhang, C. Ma, J. Xie et al., Black phosphorus/polymers: status and challenges. Adv. Mater. **33**(37), 2100113 (2021)
16. Y. Sun, J. Zhang, S. Ye et al., Progress report on property, preparation, and application of Bi_2O_2Se. Adv. Func. Mater. **30**(49), 2004480 (2020)
17. J. Wu, H. Yuan, M. Meng et al., High electron mobility and quantum oscillations in non-encapsulated ultrathin semiconducting Bi_2O_2Se. Nat. Nanotechnol. **12**(6), 530 (2017)
18. Q. Fu, C. Zhu, X. Zhao et al., Ultrasensitive 2D Bi_2O_2Se phototransistors on silicon substrates. Adv. Mater. **31**(1), 1804945 (2019)
19. H. Tang, B. Shi, Y. Wang et al., Layer-dependent photoabsorption and photovoltaic effects in two-dimensional Bi_2O_2X (X = S, Se, and Te). Phys. Rev. Appl. **15**(6), 064037 (2021)
20. K. Bu, H. Luo, S. Guo et al., Pressure-regulated dynamic stereochemical role of lone-pair electrons in layered Bi_2O_2S. J. Phys. Chem. Lett. **11**(22), 9702–9707 (2020)
21. L. Jiang, J. Li, Y. Li et al., Promoted charge separation from nickel intervening in $[Bi_2O_2]^{2+}$ layers of Bi_2O_2S crystals for enhanced photocatalytic CO_2 conversion. Appl. Catal. B **294**, 120249 (2021)
22. A.L. Pacquette, H. Hagiwara, T. Ishihara et al., Fabrication of an oxysulfide of bismuth Bi_2O_2S and its photocatalytic activity in a Bi_2O_2S/In_2O_3 composite. J. Photochem. Photobiol. A **277**, 27–36 (2014)
23. C. Huang, H. Yu, J. Chen et al., Improved performance of polymer solar cells by doping with Bi_2O_2S nanocrystals. Sol. Energy Mater. Sol. Cells **200**, 110030 (2019)
24. R. Zhang, Z. Zhou, N. Qi et al., Significant enhancement in the thermoelectric performance of Bi_2O_2S through dimensionality reduction. J. Mater. Chem. C **7**(47), 14986–14992 (2019)
25. S. Yi, X. Yue, D. Xu et al., Study on photogenerated charge transfer properties and enhanced visible-light photocatalytic activity of p-type Bi_2O_3/n-type ZnO heterojunctions. N. J. Chem. **39**(4), 2917–2924 (2015)
26. L. Xu, S. Liu, H. Zhang et al., First-principles simulation of monolayer hydrogen passivated $Bi_2O_2S_2$-metal interfaces. Phys. Chem. Chem. Phys. **22**(15), 7853–7863 (2020)
27. L. Jiang, Z. Li, D. Wang et al., In-situ growth of p-type Ag_2O on n-type Bi_2O_2S with intimate interfacial contact for NIR light-driven photocatalytic CO_2 reduction. Appl. Surf. Sci. **601**, 154185 (2022)
28. Q. Wei, C. Lin, Y. Li et al., Physics of intrinsic point defects in bismuth oxychalcogenides: a first-principles investigation. J. Appl. Phys. **124**(5), 055701 (2018)
29. X. Zhang, Y. Liu, G. Zhang et al., Thermal decomposition of bismuth oxysulfide from photoelectric Bi_2O_2S to superconducting $Bi_4O_4S_3$. ACS Appl. Mater. Interfaces. **7**(7), 4442–4448 (2015)
30. M. Wu, X.C. Zeng, Bismuth oxychalcogenides: a new class of ferroelectric/ferroelastic materials with ultra high mobility. Nano Lett. **17**(10), 6309–6314 (2017)
31. X. Li, C. Gao, H. Duan et al., Nanocrystalline TiO_2 film based photoelectrochemical cell as self-powered UV-photodetector. Nano Energy **1**(4), 640–645 (2012)
32. J. Zhou, L. Chen, Y. Wang et al., An overview on emerging photoelectrochemical self-powered ultraviolet photodetectors. Nanoscale **8**(1), 50–73 (2016)
33. B. Wang, Z. Huang, P. Tang et al., One-pot synthesized Bi_2Te_3/graphene for a self-powered photoelectrochemical-type photodetector. Nanotechnology **31**(11), 115201 (2020)
34. G. Bianca, M.I. Zappia, S. Bellani et al., Liquid-phase exfoliated GeSe nanoflakes for photoelectrochemical-type photodetectors and photoelectrochemical water splitting. ACS Appl. Mater. Interfaces. **12**(43), 48598–48613 (2020)
35. X. Ren, Z. Li, Z. Huang et al., Environmentally robust black phosphorus nanosheets in solution: application for self-powered photodetector. Adv. Func. Mater. **27**(18), 1606834 (2017)
36. G. Chen, Y. Zhou, G. Zhang et al., Flexible, self-powered Bi_2O_2Se/Graphene photoeletrochemical photodetector based on solid-state electrolytes. Ceram. Int. **47**(18), 25255–25263 (2021)
37. P. Chauhan, A.B. Patel, G.K. Solanki et al., Flexible self-powered electrochemical photodetector functionalized by multilayered tantalum diselenide nanocrystals. Adv. Opt. Mater. **9**(22), 2100993 (2021)
38. N. Liu, H. Qiao, K. Xu et al., Hydrogen terminated germanene for a robust self-powered flexible photoelectrochemical photodetector. Small **16**(23), 2000283 (2020)
39. Y. Zhang, Y. Xu, J. Guo et al., Designing of 0D/2D mixed-dimensional van der waals heterojunction over ultrathin g-C_3N_4 for high-performance flexible self-powered photodetector. Chem. Eng. J. **420**, 129556 (2021)
40. H. Qiao, X. Chen, B. Wang et al., Novel tin disulfide/graphene photoelectrochemical photodetector based on solid-state electrolytes and its performances. J. Mater. Sci.-Mater. Electron. **30**(4), 3208–3213 (2019)
41. R.J. Candal, W.A. Zeltner, M.A. Anderson, Effects of pH and applied potential on photocurrent and oxidation rate of saline solutions of formic acid in a photoelectrocatalytic reactor. Environ. Sci. Technol. **34**(16), 3443–3451 (2000)
42. C. Xing, W. Huang, Z. Xie et al., Ultrasmall bismuth quantum dots: facile liquid-phase exfoliation, characterization, and application in high-performance UV-vis photodetector. ACS Photonics **5**(2), 621–629 (2018)
43. L. Su, X. Tang, X. Fan et al., Halogenated antimonene: one-step synthesis, structural simulation, tunable electronic and photoresponse property. Adv. Func. Mater. **29**(45), 1905857 (2019)
44. Z. Xie, C. Xing, W. Huang et al., Ultrathin 2D nonlayered tellurium nanosheets: facile liquid-phase exfoliation, characterization, and photoresponse with high performance and enhanced stability. Adv. Func. Mater. **28**(16), 1705833 (2018)
45. Z. Li, H. Qiao, Z. Guo et al., High-performance photo-electrochemical photodetector based on liquid-exfoliated few-layered InSe nanosheets with enhanced stability. Adv. Func. Mater. **28**(16), 1705237 (2018)
46. D. Ma, J. Zhao, R. Wang et al., Ultrathin GeSe nanosheets: from systematic synthesis to studies of carrier dynamics and applications for a high-performance UV-Vis photodetector. ACS Appl. Mater. Interfaces. **11**(4), 4278–4287 (2019)
47. X. Ren, B. Wang, Z. Huang et al., Flexible self-powered photoelectrochemical-type photodetector based on 2D WS_2-graphene heterojunction. Flatchem **25**, 100215 (2021)
48. M.I. Zappia, G. Bianca, S. Bellani et al., Solution-processed GaSe Nanoflake-based films for photoelectrochemical water splitting and photoelectrochemical-type photodetectors. Adv. Func. Mater. **30**(10), 1909572 (2020)
49. Y. Zhou, C. Duan, Z. Huang et al., Stable flexible photodetector based on $FePS_3$/reduced graphene oxide heterostructure with significant enhancement in photoelectrochemical performance. Nanotechnology **32**(48), 485203 (2021)
50. Y. An, Z. Xing, K. Zhu et al., Anomalous photoinduced reconstructing and dark self-healing processes on Bi_2O_2S nanoplates. J. Phys. Chem. Lett. **11**(18), 7832–7838 (2020)